Reaction Mechanism of the Iron−Sulfur Flavoenzyme Adenosine-5′-Phosphosulfate Reductase Based on the Structural Characterization of Different Enzymatic States[†,‡]

Alexander Schiffer,[§,||] Günter Fritz,[§] Peter M. H. Kroneck,*[,§] and Ulrich Ermler*[,||]

Fachbereich Biologie, Mathematisch-Naturwissenschaftliche Sektion, Universität Konstanz, D-78457 Konstanz, Germany, and Max-Planck-Institut für Biophysik, Max-von-Laue-Strasse 3, D-60438 Frankfurt, Germany

Received October 24, 2005; Revised Manuscript Received January 9, 2006

ABSTRACT: The iron−sulfur flavoenzyme adenosine-5′-phosphosulfate (APS) reductase catalyzes a key reaction of the global sulfur cycle by reversibly transforming APS to sulfite and AMP. The structures of the dissimilatory enzyme from *Archaeoglobus fulgidus* in the reduced state (FAD_{red}) and in the sulfite adduct state (FAD−sulfite−AMP) have been recently elucidated at 1.6 and 2.5 Å resolution, respectively. Here we present new structural features of the enzyme trapped in four different catalytically relevant states that provide us with a detailed picture of its reaction cycle. In the oxidized state (FAD_{ox}), the isoalloxazine moiety of the FAD cofactor exhibits a similarly bent conformation as observed in the structure of the reduced enzyme. In the APS-bound state (FAD_{ox}−APS), the substrate APS is embedded into a 17 Å long substrate channel in such a way that the isoalloxazine ring is pushed toward the channel bottom, thereby producing a compressed enzyme−substrate complex. A clamp formed by residues ArgA317 and LeuA278 to fix the adenine ring and the curved APS conformation appear to be key factors to hold APS in a strained conformation. This energy-rich state is relaxed during the attack of APS on the reduced FAD. A relaxed FAD−sulfite adduct is observed in the structure of the FAD−sulfite state. Finally, a FAD−sulfite−AMP1 state with AMP within van der Waals distance of the sulfite adduct could be characterized. This structure documents how adjacent negative charges are stabilized by the protein matrix which is crucial for forming APS from AMP and sulfite in the reverse reaction.

Adenosine-5′-phosphosulfate (APS)[1] reductase (EC 1.8.99.2), ATP sulfurylase, and sulfite reductase are key enzymes in the energy metabolism of sulfate-reducing and sulfur-oxidizing microorganisms (*1*). In the pathway of dissimilatory sulfate reduction, sulfate has to be activated to APS by ATP sulfurylase at the expense of ATP; hereafter, the generated APS is cleaved and reduced to sulfite and AMP by APS reductase.

$$\mathrm{APS} + 2e^- \rightarrow \mathrm{AMP} + \mathrm{HSO_3^-}$$
$$E^{\circ\prime}(\mathrm{APS/AMP{+}HSO_3^-}) = -60\ \mathrm{mV} \quad (1)$$

Subsequently, sulfite is reduced to sulfide by sulfite reductase. Dissimilatory sulfate reduction operates under strictly anaerobic conditions and represents an important element within the sulfur cycle on earth (*3*). It is a very ancient process that has its origin ∼3 billion years ago in a hot and anoxic environment (*4*). In the sulfur-oxidizing organisms, the described pathway proceeds in the opposite direction starting from sulfide, elemental sulfur, or thiosulfate.

APS reductases from several sulfate-reducing organisms have been investigated with respect to their molecular, spectroscopic, and kinetic properties and their primary structure (*5*−*9*). The X-ray structure of APS reductase from thermophilic *Archaeoglobus fulgidus* (*10*) was recently elucidated at 1.6 Å resolution (*11*) (Figure 1). Briefly, APS reductase of *A. fulgidus* consists of two different subunits that are arranged as an $\alpha_2\beta_2$ heterotetramer. The α-subunit (molecular mass of 75 kDa) harboring the FAD cofactor can be grouped into the FAD-binding (A2−A261 and A394−A487), the helical (A488−A643), and the capping domains (A262−A393); each of them folds as an α/β structure. This overall architecture classifies APS reductase as member of the fumarate reductase family (*12*). The structure of the β-subunit (20 kDa, B1−B151) consists of a bacterial ferredoxin-like segment carrying two [4Fe-4S] clusters, a three-stranded antiparallel β-sheet, and a tail with a length of 50 Å. The global part of the β-subunit is embedded into a broad cleft of the α-subunit, while its long tail wraps around the α-subunit (Figure 1). The conversion of APS to sulfite and AMP catalyzed by APS reductase consists of an electron transfer step and an ester cleavage. Two electrons are transferred one by one from a yet unknown electron donor to the two [4Fe-4S] clusters and from there to the isoalloxazine ring of FAD via its *si*-side. The ester cleavage reaction

[†] This work is supported by the Max-Planck-Gesellschaft and the Deutsche Forschungsgesellschaft (ER 222/2-1,2; PK 451/32-3).

[‡] The structures of the FAD_{ox}−APS, FAD−sulfite−AMP1/2, FAD−sulfite, and FAD_{ox} states have been deposited in the Protein Data Bank as entries 2FJA, 2FJB, 2FJD, and 2FJE, respectively.

* To whom correspondence should be addressed. P.M.H.K.: telephone, +49-(0)7531-88-2103; fax, +49-(0)7531-88-2966; e-mail, peter.kroneck@uni-konstanz.de. U.E.: telephone, +49-(0)69-6303-1054; fax, +49-(0)69-6303-1002; e-mail, ulrich.ermler@mpibp-frankfurt.mpg.de.

[§] Universität Konstanz.

[||] Max-Planck-Institut für Biophysik.

[1] Abbreviations: APS, adenosine 5′-phosphosulfate; AMP, adenosine 5′-monophosphate; FAD, flavin adenine dinucleotide.

10.1021/bi0521689 CCC: $33.50
Published on Web 02/09/2006

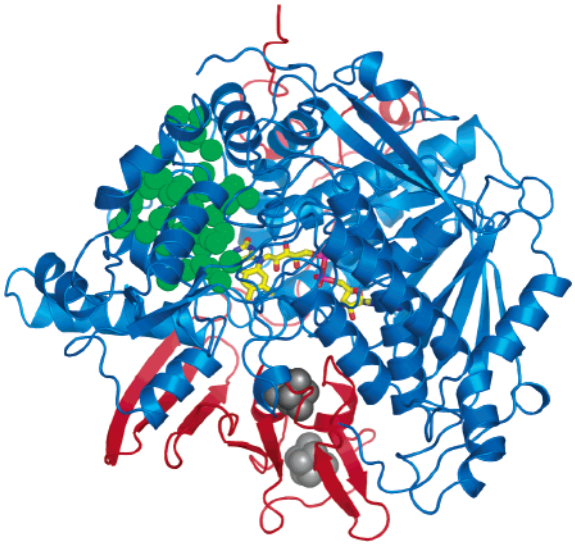

FIGURE 1: Structure of APS reductase from *A. fulgidus*. Ribbon plot of the dimer of APS reductase. The α-subunit is colored blue and the *β*-subunit red. The [4Fe-4S] clusters and FAD are shown as ball-and-stick representations. The active site channel located between the central and capping domains of the α-subunit is filled with water molecules depicted as green spheres.

is located at the *re*-side of FAD within a 17 Å long channel (Figure 1) filled with ~35 tightly bound water molecules, indicating a strong electrostatic field favorable for binding charged groups (*11*).

The reaction mechanism of APS reductase features a nucleophilic attack of the N^5 atom of reduced FAD on the sulfur of APS to form a FAD−APS intermediate which decomposes spontaneously to AMP and to the FAD−sulfite adduct. The latter is subsequently cleaved, and sulfite is finally liberated. This scenario was originally postulated by Michaels (*13*) and recently corroborated by spectroscopic and structural data (*6*, *11*). In this report, we present a detailed mechanism of APS reductase based on six enzyme structures that differ in their active sites with respect to the binding of substrates, products, and intermediates and with respect to the oxidation state of FAD.

EXPERIMENTAL PROCEDURES

Purification and Crystallization. The cultivation of *A. fulgidus* (DSM 4304T) was performed by H. Huber (Universität Regensburg, Regensburg, Germany) as previously described (*10*). APS reductase was purified and crystallized according to the method of Roth et al. (*14*). All manipulations were carried out in an anaerobic chamber (95% N_2 and 5% H_2; Coy) equipped with palladium catalyst type K-0242 (0.5% Pd/Al_2O_3; ChemPur) to remove traces of dioxygen. To analyze the binding of different substrates, intermediates, and products to the active site of APS reductase, crystals were transferred into a solution composed of 6% PEG 4000, 0.1 M NaCl, 0.1 M NaAc (pH 4.8), and 25% glycerol that also served as a cryoprotectant solution (*14*).

Data Collection. Data were collected at the Max-Planck wiggler beamline 6 (BW6) of the German electron synchrotron DESY (Hamburg, Germany) equipped with a Mar Research CCD detector. The data sets were indexed, integrated, and reduced using XDS (*15*) and HKL (*16*). For all further steps, data sets were converted with XSCALE, XDSCONV (*15*), and F2MTZ, TRUNCATE, and MTZ2VARIOUS (*17*). The statistics of the data sets are listed in Table 1.

Refinement and Structure Analysis. Protein structures were refined using standard protocols of CNS (*18*). The course of refinement was controlled by the separation of 5% of the reflections, which were only used for the R_{free} calculation (*19*). Model building and manipulation performed in O (*20*) were carried out on the basis of the $2F_o - F_c$ and $F_o - F_c$ electron density maps. The starting phases were calculated from coordinates of the FAD_{red} state (*11*). The refinement statistics of each enzymatic state are listed in Table 1. The quality of the data was assessed with CNS and PROCHECK (*21*). Rearrangements of the protein matrix in the different structures of APS reductase were identified and quantified by NCSGROUPS (Diederichs, personal communication). Figures 1−4 were created with PYMOL (DeLano Scientific), and Figure 5 was created with ChemSketch (ACD, Toronto, ON).

RESULTS

Structures of APS Reductase in Different States. To establish the enzymatic mechanism of the reduction of APS to sulfite on an atomic basis, we determined the crystal structures of six enzymatic states summarized in Figure 2. Crystals of APS reductase as isolated (FAD_{red}) were taken from the anaerobic chamber and soaked with APS, $K_3Fe(CN)_6$ and APS, AMP and sodium sulfite, sodium dithionite, and $K_3Fe(CN)_6$. The six determined structures revealed seven distinct enzyme states called FAD_{red}, FAD−sulfite−AMP, FAD_{ox}−APS, APS−sulfite−AMP1, APS−sulfite−AMP2, FAD−sulfite, and FAD_{ox} (for details, see Table 1). Both the high resolution of the data and the small differences between the crystals allow a reliable discussion of coordinate shifts on the order of 0.2 Å (Table 1). In the determined APS reductase structures, the two $\alpha\beta$ dimers in the asymmetric unit do not differ significantly from each other. However, a few differences are observed and described when they are biologically relevant.

FAD_{red} State. The structure of APS reductase was originally determined in the FAD_{red} state (*11*) which contains FAD as reduced $FADH^-$ (Figure 2). A pronounced feature of this state is a bend of the isoalloxazine ring along the N^5−N^{10} axis by an angle of 25°. Hereby, the pyrimidine and the dimethylbenzene ring of isoalloxazine are pushed to the *si*-side by the properly positioned side chains of AsnA74 and TrpA234, respectively, whereas the pyrazine ring is held in position by LeuA70 which protrudes toward the *si*-face of FAD. The most relevant polar contact between the isoalloxazine ring and the protein matrix is around the N(1)−C(2)═O group, where a positively charged surrounding contributes to the stabilization of the deprotonated pyrimidine ring (*22*).

FAD−Sulfite−AMP State. APS reductase in the FAD−sulfite−AMP state harbors a FAD−sulfite adduct and an AMP molecule with a low occupancy that could, therefore, not be unequivocally assigned (*11*). The isoalloxazine ring is again bent, and the covalently linked sulfite molecule lies outside the pyrazine ring plane and points toward the entrance of the channel. Note that this state was obtained after the crystals had been soaked with APS. This clearly indicates that the reaction proceeds within the crystal, and obviously,

Table 1: Data Collection and Refinement Statistics for Different Enzymatic States[a]

	FAD_{red}	FAD−sulfite−AMP	FAD_{ox}−APS	FAD−sulfite−AMP1/2	FAD−sulfite	FAD_{ox}
enzymatic state	E−[FADH]$^-$	E−[FADH−SO_3]$^{2-}$ with AMP (low occupancy)	E−[FAD] with APS	E−[FADH−SO_3]$^{2-}$ with AMP (two sites)	E−[FADH−SO_3]$^{2-}$	E−[FAD]
soaked compound		APS	$K_3Fe(CN)_6$ with APS	AMP with Na_2SO_3	$Na_2S_2O_4$	$K_3Fe(CN)_6$
concentration (mM)		5	5	5	5	5
time (h)		10	24	10	2	2
wavelength (Å)	1.05	1.05	1.05	1.05	1.05	1.05
resolution (Å)	1.6	2.5	2.0	1.7	1.85	1.8
completeness (%)	92.6	79.2	93.0	95.0	87.2	92.6
multiplicity	3.4	2.6	5.0	2.7	5.0	3.1
R_{sym} (%)	6.3	8.0	5.0	4.6	5.4	3.8
R_{cryst} (%)	17.6	16.0	17.7	16.8	15.7	16.6
R_{free} (%)	19.8	19.9	20.9	19.2	18.2	19.2
rmsd for bond lengths (Å)	0.010	0.008	0.010	0.007	0.007	0.009
rmsd for bond angles (deg)	1.4	1.5	1.4	1.3	1.3	1.3
rmsd from FAD_{red} (Å)	0.000	0.112	0.084	0.125	0.083	0.040
PDB entry	1JNR	1JNZ	2FJA	2FJB	2FJD	2FJE

[a] The rmsd from the FAD_{red} state was calculated for residues A2−A643 except for the FAD−sulfite−AMP1 state, where residues C2−C643 (subunit α′) were used. The crystals belong to space group $P2_12_12_1$ with the following unit cell parameters: $a = 72.4$ Å, $b = 113.2$ Å, and $c = 194.0$ Å.

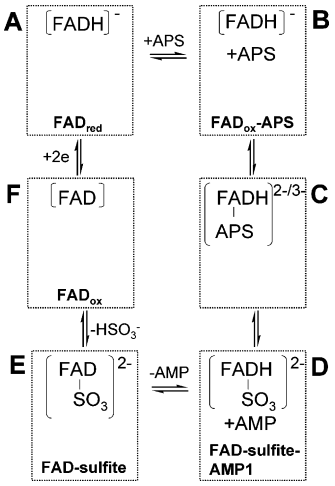

FIGURE 2: Schematic overview of the structurally characterized enzyme states combined with the postulated steps of the reaction cycle. The reaction steps are written at the top and the names of the most related APS reductase structure at the bottom of each rectangle. No structure was determined for the FAD−APS intermediate (panel C).

crystal packing effects do not substantially influence the structure in the active site region. Subtle differences in the polypeptide chain compared to the FAD_{red} structure could not be identified due to the low resolution (2.5 Å).

FAD_{ox}−APS State. When APS reductase crystals were soaked with the oxidizing agent $K_3Fe(CN)_6$ and the substrate APS, APS but not the FAD−sulfite adduct became visible in the electron density map, indicating that the reduction of APS to sulfite and AMP (leading to the FAD−sulfite−AMP state) was completely suppressed after incubation of crystalline APS reductase with ferricyanide. The APS molecule is deeply embedded in the active site channel such that solely the pyrimidine edge of its adenine ring is in contact with bulk solvent. The active site is shielded from bulk solvent (Figure 3A), but several structural water molecules are visible in the channel and play a role in substrate binding and perhaps also in catalysis.

While the conformation of the adenine and the ribose ring of APS is well-defined in the FAD_{ox}−APS state, the phosphate and, in particular, the sulfate group appear to be rather conformationally flexible. In the first conformational state present with the highest occupancy, the sulfate group is directly positioned in front of the pyrazine ring of FAD, with the distance between the sulfur and N5 atoms being ~3.4 Å. This conformation presumably corresponds to the structure of APS prior to the reaction with FAD. Interestingly, APS is not arranged in an extended manner as it contains a pronounced bulge between C8 of adenine and the phosphate O5 atoms that results in a distance between these two atoms of 3.4 Å (Figure 3A).

In the second conformational state, the sulfate group evades the pyrazine ring parallel to the isoalloxazine ring and lies in front of the dimethylbenzyl part, albeit with a larger distance. In the third conformation of APS, the sulfate group lies perpendicular to the other positions and interacts with the side chains of ArgA265 and HisA398. The presence of these catalytically unproductive conformations (they are too far from N5) is surprising but compatible with the inhibitor properties of APS at higher concentrations (*6*). All three conformations resemble that of APS found in ATP sulfurylase (*23*) but vary with respect to the position of the sulfate. Note that APS sulfurylase and APS reductase differ completely in their fold and in the interactions between APS and the polypeptide chain.

The binding affinity of APS (*6*) for APS reductase is reflected by a large number of protein−substrate interactions (Figure 3A). The sulfate O1 atom interacts with the ND2 atom of AsnA74, its O2 atom with the NE2 atom of HisA389, and its O3 atom via a water molecule with ArgA265 and TrpA234 and via two water molecules with GluA141, AspA361, and AsnA74. Additionally, ArgA265 is hydrogen bonded to the O3A atom that links the sulfate and phosphate groups. The phosphate oxygen atoms are connected to ArgA265 via a salt bridge and to the peptide nitrogens of ValA273 and GlyA274, located at the positively charged N-terminus of helix α6. The hydroxyl group O2 of ribose is linked to the side chain hydroxyl group of TyrA95 and that of O3 to HisA446 and TyrA95 via a water molecule. The fixation of the adenine ring of APS is mainly ac-

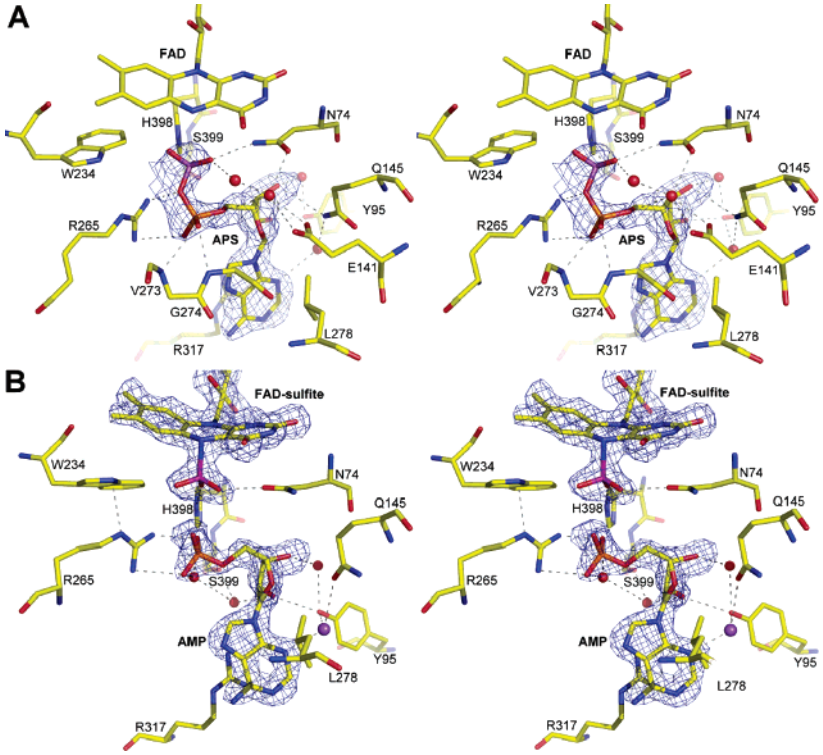

FIGURE 3: Stereoview of the structure of APS reductase in the FAD_{ox}−APS (A) and FAD−sulfite−AMP1 (B) states. The electron density is contoured at 1σ. (A) APS binds in a curved conformation to the prebuilt channel. Invariant residues HisA398, AsnA74, and ArgA265 play a key role in phosphosulfate binding and catalysis. The adenine part is firmly clamped between LeuA278 and ArgA317, and the latter swings into the channel upon substrate binding. (B) This state contains a FAD−sulfite adduct and AMP, the latter adopting a conformation similar to the AMP moiety of APS. This structure shows how the phosphate of AMP and the sulfite of the FAD−sulfite adduct (both negatively charged) are kept in van der Waals contact.

complished by sandwiching it between LeuA278 and ArgA317 whereby the coplanar arrangement of the guanidinium group is optimal for $\pi-\pi$ interactions (Figure 3A). Additionally, one polar contact is formed between the N3 atom of the adenine ring and the protein mediated by a solvent molecule (see the next section).

The most striking structural difference between the FAD_{ox}−APS and FAD_{red} state is the large conformational change in ArgA317. In the substrate-free state, the guanidinium group is directed toward the bulk solvent ("arginine out"). Once APS binds, it swings into the channel and aligns in the described coplanar fashion ("arginine in"). The distance for the guanidine NH2 atom between arginine in and out is 6.1 Å. While the side chain of ArgA317 is rather flexible and not stabilized by hydrogen bonds in the arginine out position, it is strongly anchored to AMP as well as to the carbonyl oxygen atom of IleA312 and the hydroxyl group of ThrA314 in the arginine in position. ThrA314 evades the incoming AMP and ArgA317 by around 0.3 Å.

The binding of APS at the *re*-side of FAD induces a conformational change in the isoalloxazine ring. In comparison to the FAD_{red} structure, the isoalloxazine ring and the ribityl group are rotated ~10° around an axis that crosses all three macrocyclic rings and is shifted ~0.4 Å toward the channel bottom. This rotation results in a shift of the lower part of the pyrazine and the dimethylbenzene ring of ~0.6 Å away from the sulfate of APS (Figure 4). The backstop residue LeuA70 propagates the shift of the isoalloxazine ring and induces at the *re*-face of FAD a small conformational change over a larger region that also reaches [4Fe-4S] cluster I via TrpB48 and CysB47, the latter being a ligand of [4Fe-4S] cluster I. Whether these minor alterations have a significant effect on the redox potential of the Fe−S cluster, or its properties for electron transfer to FAD, remains an open question.

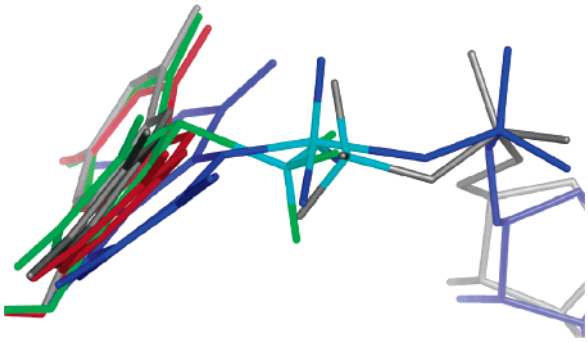

FIGURE 4: Conformations of the isoalloxazine rings in the FAD_{red} (red), FAD−sulfite (green), and FAD_{ox}−APS (gray) states after superimposition of the corresponding structures. The pentavalent highly unstable FAD−APS transition state (blue) was modeled. In all states, the sulfur atom is colored cyan. The postulated in-line sulfite transfer mechanism is derived from the arrangement of the sulfotrioxide part of APS and sulfite in the FAD_{ox}−APS and FAD−sulfite states. The aligned isoalloxazine rings visualize their distinct conformations reflecting strained and relaxed states. The N−S bond length in the FAD−sulfite state is 2.05 Å. The positions of the sulfurs in the FAD−sulfite and FAD_{ox}−APS states are 0.6 Å apart.

FAD−Sulfite−AMP1 and FAD−Sulfite−AMP2 States. The addition of sulfite and AMP to APS reductase crystals results in two substantially different states denoted as FAD−sulfite−AMP1 and FAD−sulfite−AMP2 states. Whereas the first α-subunit of the asymmetric unit essentially contains the FAD−sulfite−AMP1 state, the second α-subunit harbors

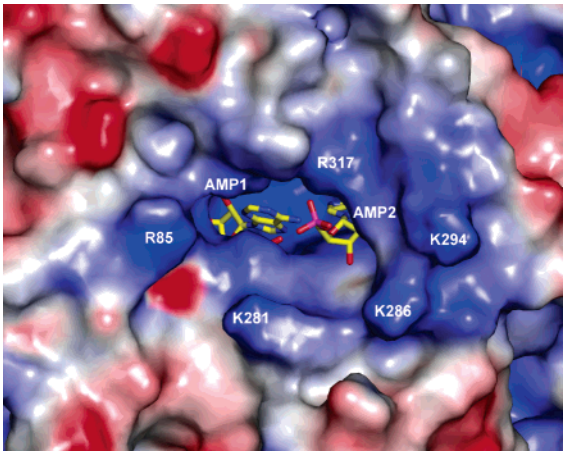

FIGURE 5: Electrostatic surface representation of the channel region, including the distal and proximal binding site of APS and AMP. The entrance of the channel is surrounded by four positively charged residues that can attract negatively charged substances such as APS or AMP. Areas with positive and negative electrostatic potentials are colored blue and red, respectively.

AMP predominantly in the FAD−sulfite−AMP2 state (Figures 3B and 5). The different binding modes of AMP also influence the conformation of the FAD−sulfite adduct.

AMP in the FAD−sulfite−AMP1 state is bound to the so-called proximal binding site in the vicinity of FAD (Figures 2 and 3B) and very similar to the AMP moiety of APS in the FAD−APS state. However, because of the higher resolution and the decreased conformational flexibility of AMP compared to APS, the protein−ligand interactions can be described more accurately. The N1, N3, and N7 atoms of the adenine ring are tied to the polypeptide chain mediated by solvent molecules (Figure 3B). The high electron density in front of the N3 atom was tentatively assigned to a sodium ion. This putative sodium ion is coordinated to TyrA95, GlnA145, and a water molecule, the latter being connected to the backbone nitrogen of GlnA143. The only larger difference between AMP and the AMP moiety of APS in the FAD_{ox}−APS state is a 1.3 Å shift of the phosphate group. This displacement does not change the binding partners but the distance to them. Phosphate atoms O1 and O2 and the guanidinium group of Arg265 form a strong bidentate salt bridge with O−N distances of 2.5 and 2.9 Å, respectively (Figure 3B). Atom O3 loosely interacts with HisA389, ValA273, and GlyA274, the latter two residues being located at the N-terminal end of helix α6 (Figure 3B). Helix α6 is shifted 0.4 and 0.2 Å toward the phosphate group compared to that in the FAD_{red} and FAD_{ox}−APS states, respectively, thereby enhancing these interactions.

Compared to the FAD_{red} state, the isoalloxazine ring and the ribityl chain are rotated and translated in a related fashion as found in the FAD_{ox}−APS state such that the ribityl group remains roughly at its position and the lower part of the isoalloxazine ring moves toward the channel bottom. The contacting residues correspond to those described for the sulfate group of APS in the FAD_{ox}−APS state. Only ArgA265 is not directly hydrogen bonded to the sulfite and participates in stabilization of the negatively charged phosphate group of AMP.

In the FAD−sulfite−AMP2 state, AMP is bound to the distal binding site (Figure 5) and roughly 5 Å from the proximal binding site. In the distal binding site, the adenine ring is accommodated in a hydrophobic pocket close to the channel entrance formed by Phe264, Phe277, Tyr292, Val321, and the hydrophobic part of Arg317 (Figure 5). The ribose and phosphate groups point either toward the bulk solvent or toward the proximal binding site, but their electron densities are not sufficiently defined to allow for further structural details. Notably, in the second α-subunit, the side chain of Arg317 is mainly located in an arginine out position, also documenting the predominant existence of the FAD−sulfite−AMP2 state. The structure of the FAD−sulfite adduct presumably corresponds to that of the FAD−sulfite state described below.

FAD−Sulfite State. APS reductase crystals soaked with the reducing agent sodium dithionite lead to the FAD−sulfite state, which again contains the FAD−sulfite adduct (Figure 2). This adduct could be formed since APS reductase is partly oxidized during the soaking process and subsequently reacts with sulfite, which is usually present in sodium dithionite.

Compared to the FAD_{red} state, the isoalloxazine ring in the FAD−sulfite state undergoes a similar rotational movement as observed in the FAD_{ox}−APS and FAD−sulfite−AMP1 states, but without the concomitant shift toward the channel bottom (Figure 4). This minor displacement of the isoalloxazine ring between the FAD−sulfite and FAD_{red} states did not significantly affect the position of atom N5 but did affect the direction of the N5−S bond. Interestingly, the sulfite conformation in the FAD−sulfite state deviates from that in the FAD−sulfite−AMP1 state as the sulfite oxygens are rotated by ∼35° around the N5−S bond. The residues that are hydrogen bonded to the sulfite oxygens are identical except for the additional ArgA265 in the FAD−sulfite state. The electron density at the sulfate oxygens in the FAD_{ox}−APS state is of insufficiently good quality to allow a definition of their accurate position.

Except for small rearrangements of HisA389 and ArgA265 on the order of 0.4 Å to optimize the hydrogen bonds to the sulfite oxygens, the structures of the FAD_{red} and FAD−sulfite states superimpose nearly perfectly, with all deviations being less than 0.2 Å. In addition to local side chain adjustments, APS and AMP binding is accompanied by long-range conformational changes in the surroundings of the active site.

FAD_{ox} State. APS reductase in the oxidized state FAD_{ox} (Figure 2) revealed a structure nearly identical to that of the FAD_{red} state. Surprisingly, even the isoalloxazine ring system is found in the same conformation as in the FAD_{red} state, although a more coplanar orientation of the three aromatic rings would be energetically favorable in the oxidized state (*24*, *25*). For example, thioredoxin reductase adopts a roughly planar conformation in the oxidized state and a bent conformation (bending angle of 34°) in the reduced state (*26*). Obviously, in APS reductase, Leu70, Asn74, and Trp234 are sufficiently fixed to maintain the so-called butterfly conformation independent of the redox state of the FAD cofactor (*11*).

The only significant differences in the active site region between the FAD_{red} and FAD_{ox} states were observed for residues MetA365 and ThrA366. The methyl group of MetA365 moves 0.6 Å toward the N5 atom of FAD, presumably to fill the empty space left after deprotonation at the N5 atom. As a consequence, the OG1 atom of ThrA366 also slightly moves toward the FAD. This finding also

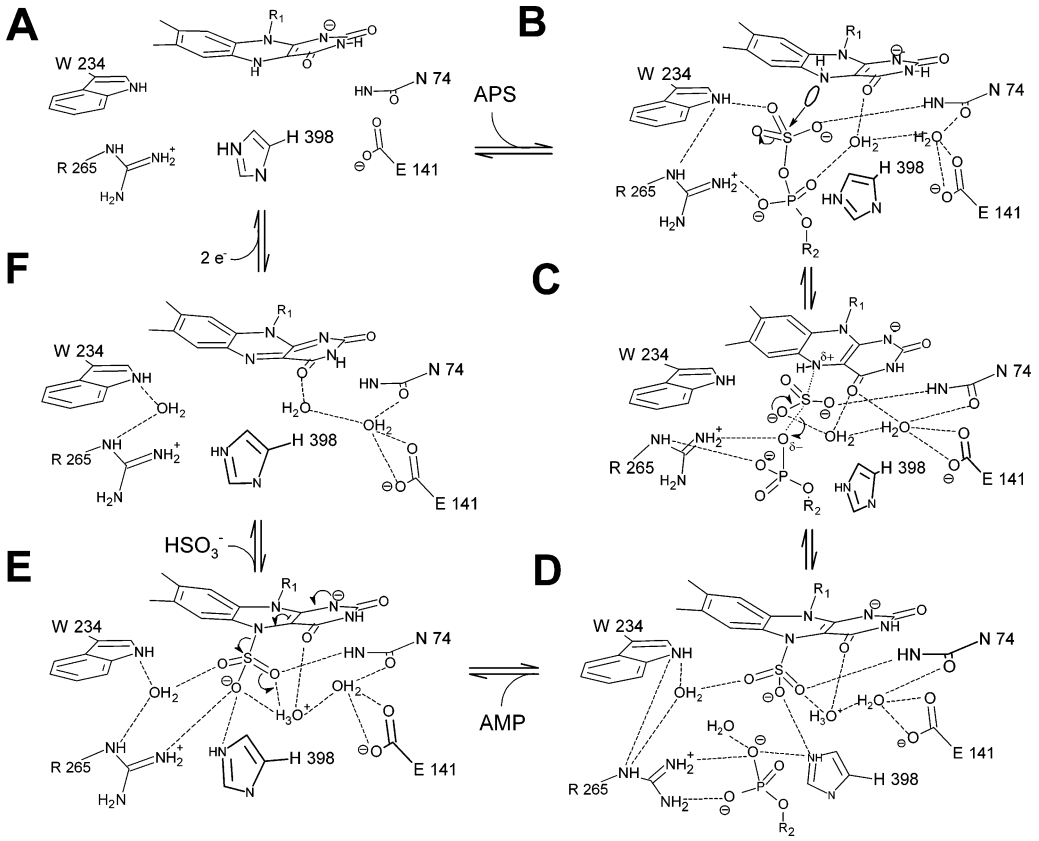

FIGURE 6: Reaction cycle of APS reductase. From six enzyme states (A−F) along the reaction pathway, five were structurally characterized: (A) FAD reduced (FAD_{red} state), (B) FAD reduced with APS bound (note that in the crystal structure FAD is oxidized, FAD_{ox}−APS state), (D) sulfite adduct with AMP bound (FAD−sulfite−AMP1 state), (E) sulfite adduct (FAD−sulfite state), and (F) oxidized FAD (FAD_{ox} state). (C) The postulated short-lived FAD−APS intermediate was modeled.

supports the assumption that the flavin moiety is not significantly reduced by synchrotron radiation during data collection.

DISCUSSION

Substrate Binding. The analysis of the enzymatic states clearly documents that the channel in APS reductase is prebuilt in the substrate-free state. In contrast to the structurally related fumarate reductases (*27*), a relative movement between the central and capping domains (both forming the channel) is prevented in APS reductase by an increased number of interactions between these domains and between the α- and *β*-subunits (Figure 1). However, substrate binding induces small conformational changes in the active site region that are transmitted over larger distances within the protein matrix.

Unexpectedly, the crystallographic data of APS reductase offer detailed insights into the process of substrate binding. First, the substrate is recognized by a patch of positively charged residues (ArgA83, LysA281, LysA283, and ArgA317) at the entrance of the substrate channel that attracts negatively charged molecules such as APS and AMP (Figure 5). Second, the adenine ring of the incoming APS molecule loosely binds to a hydrophobic pocket, the so-called distal substrate binding site. Third, the phosphosulfate group which initially points toward the bulk solvent rotates toward the channel interior and might pull with it the positively charged guanidine group of ArgA317. Fourth, in the new position, the guanidinium group of ArgA317 attracts the nearby, loosely bound adenine ring, thereby triggering the displacement of APS or AMP from the distal to the energetically favorable proximal binding site (Figure 5).

FAD−APS Transition State. Both in the forward and in the back reaction catalyzed by APS reductase, the formation of the short-lived FAD−APS transition state is most likely the rate-limiting step (Figure 2).

In the forward reaction, the orbitals of the negatively charged sulfate oxygen atoms and the electron-rich isoalloxazine ring must overlap slightly to position the N5 atom of FAD and the sulfate sulfur atom optimally for a nucleophilic attack (Figure 4). Interestingly, orbital overlapping and concomitantly the binding and activation energy become reduced because of the butterfly shape of the isoalloxazine ring with N5 of the pyrazine being directed to and the wings away from the substrate. The FAD_{ox}−APS structure revealed a van der Waals distance of 3.4 Å between the nitrogen and sulfur atoms accompanied by a shift of the isoalloxazine ring and the protein wall at the channel bottom of ∼0.6 Å (Figure 4) away from the arriving APS. Obviously, APS binding exerts a pressure on the isoalloxazine ring, thereby causing a strained conformation of the isoalloxazine ring, parts of the polypeptide chain, and APS. ArgA317 might play a key role by fixing the adenine ring and the "tense spring"-like conformation of APS. Substrate distortion and destabilization of substrate binding in general will increase the energy of the enzyme−substrate complex which is an important mechanism for rate enhancement used by many biological catalysts (*28*−*30*).

The back reaction proceeds by a nucleophilic attack of the charged phosphate oxygen on the sulfur of the sulfate

anion. As observed in the FAD−sulfite−AMP1 state, the FAD−sulfate adduct is again in a strained conformation (Figure 3B) when the reactants are brought within van der Waals distance. Similar to the arginine in kinases (*31*), ArgA265 plays a major role in charge compensation and in the proper orientation of the charged groups. However, in nucleotide kinases, the reaction proceeds by a clash between the two negatively charged substrates due to a long-range conformational change of two subdomains (*32*), whereas in APS reductase, the substrates are compressed in a prebuilt active site.

The structures of the FAD_{ox}−APS and FAD−sulfite states suggest an in-line transfer mechanism for the sulfuryl transfer (Figure 4) that is also in agreement with that of the sulfotransferase reaction (*33*, *34*). It is unknown whether the sulfonation reaction of APS reductase proceeds by an associative or dissociative reaction. From a structural point of view, an associative mechanism is more likely as the increased negative charge on the sulfate oxygens can be compensated by the protein matrix and the strained conformations of FAD and APS (or FAD−sulfite adduct and AMP in the back reaction) become more relaxed. Accordingly, the N5 atom shifts ∼0.6 Å toward the sulfate sulfur atom as observed in the relaxed conformation of the FAD−sulfite state. Simultaneously, the attracted sulfate sulfur atom moves ∼0.6 Å toward the N5 atom to be exactly located in the center of the trigonal bipyramidal FAD−APS transition state (Figure 4). The length of the covalent N−S bond is now ∼2.1 Å. This value corresponds fairly well to the observed N−S distance of 2.05 Å in the FAD−sulfite state (Figure 4). The displacement of the sulfate sulfur atom keeps the position of the AMP moiety of APS essentially unchanged and might lead to a relaxation of APS. Note that the reaction takes place without displacement of the sulfate oxygens by more than 1 Å and without breakage of a hydrogen bond to the mentioned hydrogen donors.

Structure-Based Catalytic Cycle. A catalytic cycle is outlined on the basis of the described structures of the enzymatic states (Figures 2 and 6). After APS binds, the sulfonation reaction proceeds by an in-line attack of the nucleophile N5 of FAD on the sulfate sulfur of APS. Catalysis is supported by an increase in the nucleophilicity of N5 due to the deprotonated N1 atom and of the electrophilicity of the sulfur due to hydrogen bonds between the four sulfate oxygens of APS and AsnA74, TrpA234, ArgA265, and HisA398 (*11*). In contrast to sulfotransferase (*33*) which also catalyzes a sulfuryl transfer reaction, no proteinogenic hydrogen acceptor is present adjacent to the N5H atom of FAD. Therefore, the proton might be transferred from N5 of FAD to O2B of the sulfate of APS within a four-atom center and then passed to AMP or alternatively via two water molecules to side chains of AsnA74, GluA141, and AspA361. These residues are, however, not strictly conserved in the so far known APS reductase sequences (data not shown). Transfer of a proton to the NE2 atom of HisA398 is unlikely as the NE2 atom is already protonated because of hydrogen bonds to the sulfate sulfur (Figure 6). The postulation of the sulfate as a proton transmitter requires a short-lived FAD−APS intermediate within an associative mechanism. A sulfotrioxide-like transition state within a dissociative mechanism cannot accept a proton. Substrate-induced catalysis involving proton abstraction is also discussed for $p21^{ras}$ (*35*) and glutaminyl-tRNA synthetase (*36*).

The sulfonation reaction receives additional support from the protein environment as the two charges of the phosphate group of the released AMP are efficiently compensated (Figure 3B). The subsequent dissociation of the FAD−sulfite adduct to yield oxidized FAD and sulfite might be enzymatically assisted by protonation of the sulfite moiety, for example, via HisA398. Interestingly, the FAD−sulfite adduct which is unstable in solution ($K_d \approx 2$ M) (*37*) is thermodynamically fairly stable within the enzyme since the same molecular features that decrease the energy of the FAD−APS transition state will stabilize the FAD−sulfite adduct. Suitable molecular surroundings for stabilizing a FAD−sulfite adduct were also found in other flavoenzymes (*38*). Finally, the product sulfite is released and oxidized FAD reduced via the two [4Fe-4S] clusters (Figures 2 and 6).

ACKNOWLEDGMENT

We thank Hartmut Michel for continuous support, Sandro Ghisla for fruitful discussions, Harald Huber and Karl O. Stetter for providing us with *A. fulgidus* cells, Annette Roth for help during crystallization, and the staff of Max-Planck beamline BW6 at DESY for assistance during data collection.

REFERENCES

1. Hansen, T. A. (1994) Metabolism of sulfate-reducing prokaryotes, *Antonie van Leeuwenhoek 66*, 165−185.
2. Thauer, R. K., Jungermann, K., and Decker, K. (1977) Energy conservation in chemotrophic anaerobic bacteria, *Bacteriol. Rev. 41*, 100−180.
3. Peck, H. D., Jr., and LeGall, J., Eds. (1994) Inorganic Microbial Sulfur Metabolism, *Methods in Enzymology*, Vol. 243, Academic Press, San Diego.
4. Wagner, M., Roger, A. J., Flax, J. L., Brusseau, G. A., and Stahl, D. A. (1998) Phylogeny of dissimilatory sulfite reductases supports an early origin of sulfate respiration, *J. Bacteriol. 180*, 2975−2982.
5. Lampreia, J., Pereira, A. S., and Moura, J. J. G. (1994) Adenylylsulfate reductase from sulfate-reducing bacteria, *Methods Enzymol. 243*, 241−260.
6. Fritz, G., Büchert, T., and Kroneck, P. M. H. (2002) The function of the [4Fe-4S] clusters and FAD in bacterial and archaeal adenylylsulfate reductases. Evidence for flavin-catalyzed reduction of adenosine 5′-phosphosulfate, *J. Biol. Chem. 277*, 26066−26073.
7. Hipp, W. M., Pott, A. S., Thum-Schmitz, N., Faath, I., Dahl, C., and Trüper, H. G. (1997) Towards the phylogeny of APS reductases and sirohaem sulfite reductases in sulfate-reducing and sulfur-oxidizing prokaryotes, *Microbiology 143*, 2891−2902.
8. Klenk, H.-P., et al., and Venter, J. C. (1997) The complete genome sequence of the hyperthermophilic, sulphate-reducing archaeon *Archaeoglobus fulgidus*, *Nature 390*, 364−370.
9. Dahl, C., and Trüper, H. G. (2001) Sulfite Reductase and APS Reductase from *Archaeoglobus fulgidus*, *Methods Enzymol. 331*, 472−441.
10. Stetter, K. O., Lauerer, G., Thomm, M., and Neuner, A. (1987) Isolation of extreme thermophilic sulfate reducers: Evidence for a novel branch of archaebacteria, *Science 236*, 822−824.
11. Fritz, G., Roth, A., Schiffer, A., Büchert, T., Bourenkov, G., Bartunik, H. D., Huber, H., Stetter, K. O., Kroneck, P. M. H., and Ermler, U. (2002) Crystal structure of the adenylylsulfate reductase from the hyperthermophilic Archaeon *Archaeoglobus fulgidus* at 1.6 Å resolution, *Proc. Natl. Acad. Sci. U.S.A. 99*, 1836−1841.
12. Lancaster, C. R. D. (2003) *Wolinella succinogenes* quinol:fumarate reductase and its comparison to *E. coli* succinate:quinone reductase, *FEBS Lett. 555*, 21−28.
13. Michaels, G. B., Davidson, J. T., and Peck, H. D., Jr. (1970) A flavin-sulfite adduct as an intermediate in the reaction catalyzed by adenylyl sulfate reductase from *Desulfovibrio vulgaris*, *Biochem. Biophys. Res. Commun. 39*, 321−328.
14. Roth, A., Fritz, G., Büchert, T., Huber, H., Stetter, K. O., Ermler, U., and Kroneck, P. M. H. (2000) Crystallization and preliminary

X-ray analysis of adenylylsulfate reductase from *Archaeoglobus fulgidus*, *Acta Crystallogr. D56*, 1673−1675.
15. Kabsch (1993) Automatic processing of rotation diffraction data from crystals of initially unknwon symmetry and cell constants, *J. Appl. Crystallogr. 26*, 795−800.
16. Otwinowski, Z., and Minor, W. (1996) Processing of X-ray diffraction data collected in oscillation mode, *Methods Enzymol. 276*, 307−326.
17. Collaborative Computational Project Number 4 (1994) The CCP4 Suite: Programs for protein crystallography, *Acta Crystallogr. D50*, 760−763.
18. Brünger, A., et al., and Warren, G. L. (1998) Crystallography and NMR system: A new software suite for macromolecular structure determinations, *Acta Crystallogr. D54*, 905−921.
19. Brünger, A. T. (1992) Free *R* value: A novel statistical quantity for assessing the accuracy of crystal structures, *Nature 355*, 472−475.
20. Jones, T. A., Zou, J. Y., Cowan, S. W., and Kjeldgaard, M. (1991) Improved methods for building protein models in electron density maps and the location of errors in these models, *Acta Crystallogr. A47*, 110−111.
21. Laskowski, R. A., MacArthur, M. W., Moss, D. S., and Thornton, J. M. (1993) PROCHECK: A program to check the stereochemical quality of protein structures, *J. Appl. Crystallogr. 26*, 283−291.
22. Ghisla, S., and Massey, V. (1986) New flavins for old: Artificial flavins as active site probes of flavoproteins, *Biochem. J. 239*, 1−12.
23. Ullrich, T. C., Blaesse, M., and Huber, R. (2001) Crystal structure of ATP sulfurylase from *Saccharomyces cerevisae*, a key enzyme in sulfate activation, *EMBO J. 20*, 316−329.
24. Dixon, D. A., Lindner, D. L., Branchaud, B., and Lipscomb, W. N. (1979) Conformations and electrostatic structures of oxidized and reduced isoalloxazine, *Biochemistry 18*, 5770−5775.
25. Hall, L. H., Bowers, M. L., and Durfor, C. N. (1987) Further consideration of flavin coenzyme biochemistry afforded by geometry-optimized molecular orbital calculations, *Biochemistry 26*, 7401−7409.
26. Lennon, B. W., Williams, C. H., and Ludwig, M. L. (1999) Crystal structure of refined thioredoxin reductase from *Escherichia coli*: Structural flexibility in the isoalloxazine ring of the flavin adenine dinucleotide cofactor, *Protein Sci. 8*, 2366−2379.
27. Bamford, V., Dobbin, P. S., Richardson, D. J., and Hemmings, A. M. (1999) Open conformation of a flavocytochrome c_3 fumarate reductase, *Nat. Struct. Biol. 6*, 1104−1107.
28. Narlikar, G. J., Gopalakrishnan, V., McConnell, T. S., Usman, N., and Herschlag, D. (1995) Use of binding energy by an RNA enzyme for catalysis by positioning and substrate destabilization, *Proc. Natl. Acad. Sci. U.S.A. 92*, 3668−3672.
29. Sidhu, G., Withers, S. G., Nguyen, N. T., McIntosh, L. P., Ziser, L., and Brayer, G. D. (1999) Sugar ring distortion in the glycosyl-enzyme intermediate of a family G/11 xylanase, *Biochemistry 38*, 5346−5354.
30. Gil-Ortiz, F., Ramón-Maiques, S., Fita, I., and Rubio, V. (2003) The course of phosphorus in the reaction of *N*-acetyl-L-glutamate kinase, determined from the structures of crystalline complexes, including a complex with an AlF_4^- transition state mimic, *J. Mol. Biol. 331*, 231−244.
31. Lavie, A., Konrad, M., Brundiers, R., Goody, R. S., Schlichting, I., and Reinstein, J. (1998) Crystal structure of yeast thymidylate kinase complexed with the bisubstrate inhibitor P1-(5′-adenosyl) P5-(5′-thymidyl) pentaphosphate (TP5A) at 2.0 Å resolution: Implication for catalysis and AZT activation, *Biochemistry 37*, 3677−3686.
32. Müller, C. W., Schlauderer, G. J., Reinstein, J., and Schulz, G. E. (1996) Adenylate kinase motions during catalysis: An energetic counterbalancing substrate binding, *Structure 4*, 147−156.
33. Negeshi, M., Pederson, L. G., Petrotchenko, E., Shevtsov, S., Gorokhov, A., Kakuta, Y., and Pedersen, L. (2001) Structure and function of sulfotransferases, *Arch. Biochem. Biophys. 390*, 149−157.
34. Chapman, E., Best, M. D., Hanson, S. R., and Wong, C.-H. (2004) Sulfotransferases: Structure, mechanism, biological activity, inhibition and synthetic utility, *Angew. Chem., Int. Ed. 43*, 3526−3548.
35. Schweins, T., Geyer, M., Scheffzek, K., Warshel, A., Kalbitzer, H. R., and Wittinghofer, A. (1995) Substrate-assisted catalysis as a mechanism for GTP hydrolysis of $p21_{ras}$ and other GTP-binding proteins, *Nat. Struct. Biol. 2*, 36−44.
36. Perona, J., Rould, M. A., and Steitz, T. A. (1993) Structural basis for transfer RNA aminoacylation by *Escherichia coli* glutaminyl-tRNA synthetase, *Biochemistry 32*, 8758−8771.
37. Müller, F., and Massey, V. (1969) Flavin-sulfite complexes and their structures, *J. Biol. Chem. 244*, 4007−4016.
38. Massey, V., Müller, F., Feldberg, R., Schuman, M., Sullivan, P. A., Howell, L. G., Mayhew, S. G., Matthews, R. G., and Foust, G. P. (1969) The reactivity of flavoproteins with sulfite. Possible relevance to the problem of oxygen reactivity, *J. Biol. Chem. 244*, 3999−4006.

BI0521689